IMA Journal of Applied Mathematics (2002) **67**, 419–439

Modelling thermal front dynamics in microwave heating

GEMA A. MERCADO†
School of Mathematics, Georgia Institute of Technology, Atlanta, GA 30332, USA
and
Facultad de Matemáticas, Universidad Autónoma de Zacatecas, Zacatecas, Zac. 98068, México

BENJAMIN P. LUCE‡
Theoretical Division, Los Alamos National Laboratory, Los Alamos, NM 87545, USA

AND

JACK XIN§
Department of Mathematics and TICAM, University of Texas at Austin, Austin, TX 78712, USA

[Received on 19 July 2000; revised on 6 December 2001]

The formation and propagation of thermal fronts in a cylindrical medium that is undergoing microwave heating is studied in detail. The model consists of Maxwell's wave equation coupled to a temperature diffusion equation containing a bistable nonlinear term.

When the thermal diffusivity is sufficiently small the leading-order temperature solution of a singular perturbation analysis is used to reduce the system to a *free boundary problem*. This approximation is then used to derive predictions for the steady-state penetration and profiles of the temperature and electric fields. These solutions are valid for arbitrary values of the electric conductivity, and thus extend the previous (small conductivity) results found in the literature.

A quasi-static approximation for the electric field is then used to obtain an ordinary differential equation for the relaxation dynamics to the steady state. This equation appears to accurately describe the time scale of the electric field's evolution both with and without the presence of a strongly coupled temperature front, and may be of wider interest than the model for microwave heating studied here.

Keywords: front dynamics; Maxwell's wave; microwave heating; thermal fronts.

1. Introduction

When electromagnetic radiation interacts with matter at the proper electric and thermal parameters, it can be absorbed and hence generate heat. This principle has greatly contributed to the development of modern industry. According to Meredith (1998), heating has been the most common process used in the manufacturing industry in the last 50 years. Yet it remains one of the most difficult industrial processes to control.

†Email: gema@mate.reduaz.mx
‡Email: luceb@lanl.gov
§Email: jxin@math.utexas.edu

Electrical volumetric heating (EVH) is a relatively new process with many advantages over conventional methods based on radiation, convection and conduction. In comparison, the latter are slow and imprecise. Traditionally, a material is heated by convection on its surface, and heat is transferred to the interior by conduction. In contrast, with EVH the bulk of the material is evenly warmed. According to Meredith (1998), the processing times required by EVH are often less than one per cent of those required by traditional techniques. In addition, EVH is precise, safe, and environmentally clean. As a result, EVH has undergone a dramatic development in the later twentieth century, being now widely used in industry, medicine, and commerce.

A particular form of EVH is *microwave heating* which is based on the physical effect of bipolar polarization. When an electric field is applied to materials with high resistivity, the dipole moments of the molecules align themselves with the field. High-intensity radiation can also induce dipole moments. Because the microwave field is alternating in time, the dipoles attempt to follow the field reversals, and thus are in a constant state of oscillation, so that heat is generated. A secondary source of heat is the conduction of ionic charge induced by the field, and even very small currents can generate significant amounts of heat. Typically, microwave heating is performed at frequencies between 900 and 2450 MHz. However, values close to the upper bound are avoided because they overlap ranges of frequencies used for communications.

Microwave heating has a variety of uses in the food industry: thawing, continuous baking, vacuum drying, pasteurization, etc. It is also widely employed in health-related professions: blood flow measurements, microwave imaging, detection and treatment of cancer tumors, etc. Moreover, microwave heating is being used in environmental cleanup efforts to treat infectious medical waste, contaminated soils, nuclear waste, and sewage/waste water (Beatty *et al.*, 1992).

Despite the increasing interest and diversification of the uses of microwave heating, the highly complicated nonlinear nature of the light–matter interaction has produced an electroheat industry that mostly utilizes experimentation and speculation. However, empirical studies of many complex situations in microwave heating have proven to be an expensive approach with limited impact and success. In particular, to characterize and control unwanted regions of high temperatures based on a trial and error approach is not just impractical but irrealizable when high temperatures can rapidly form and destroy the material.

Consequently, at this time, the almost unlimited potential of electromagnetic heating stands to benefit from better theoretical development in the understanding, modelling, and control of the many associated phenomena.

One of the most common consequences of the nonlinear nature of this heating process present in the electroheat industry is an instability that causes uncontrollable and sudden increases in temperature in response to small increases in electric power. When such a thermal instability is spatially localized, some regions inside the material develop much higher temperatures with respect to the surrounding material. These regions behave as thermal fronts that can form and propagate over substantial distances inside the material, eventually relaxing into a steady-state temperature profile. In particular, a localized region of high temperature with zero temperature in its surroundings is called a hotspot. In general, the presence of thermal fronts can be beneficial, for example, the joining or smelting of ceramics or the production of specialized metal alloys, or highly undesirable if uniform

heating is required, for example, when density homogenization is sought. Consequently, it is of great practical interest to gain more understanding of the formation and dynamics of thermal fronts.

1.1 *Previous work*

There have been two main approaches to modelling thermal fronts in microwave heating. The first focuses on the thermal aspects, and utilizes only a heat equation with a nonlinear source term assuming constant magnitude of the electric field. The second and more realistic approach takes into account the spatial variation of the electric field, and hence involves Maxwell's wave equation in addition to the nonlinear heat equation.

The works of Kriegsmann, Brodwin & Watters (1990), Coleman (1990), Hill & Smyth (1990) and Tian (1991, pp. 283–300) are recognized as the seminal efforts in the field of mathematically modelling formation and propagation of hotspots in microwave heating.

The first work formulates a time-harmonic, steady-state problem for the modelling of the microwave heating of a semi-infinite ceramic half-space. The steady-state solutions are present in the form of coupled ordinary differential equations describing both the temperature distribution and the exponential decay of the electric field. A multiscale analysis produces the leading-order solutions for the cases of constant conductivity and negligible radiative losses and also for the most general case of arbitrary electrical conductivity. Their results show that the temperature increases, on a length scale that is large compared to a wavelength, from its surface value to a finite value at infinity. Kriegsmann *et al*. (1990) also conclude that the value of the temperature at infinity depends monotonically on the incident power level and that the electric field decays on the same scale as the temperature changes but oscillates rapidly on the spatial scale determined by a wavelength. This is one of the first works where a multivalued function of the incident power for temperature is analysed in relation to the stabilizing effects of electrical conductivity on thermal runaway phenomena. This work preceded others on the topic and was distilled from David Watters (1989).

Three of the other studies mentioned above assume that the intensity of the electric field is constant. These works are limited to the study of a heat conduction problem described by partial differential equation under various assumptions for the nonlinear term and also for different geometrical scenarios.

Smyth (1990) analyses microwave heating of materials with small thermal diffusivity. He presents a systematic derivation of a coupled system of equations that governs this process. The system is solved for a linear conducting medium using an asymptotic approximation for small thermal diffusivity and geometric optics for the wave equation describing the electric field. This work does not address the particular issue of thermal fronts. However, using the same derivation and model, Pincombe & Smyth (1991, pp. 479–498) find criteria for the formation of hotspots.

In the last decade, Kriegsmann made an important contribution to this field by investigating the complex dynamics of microwave heating. He focused on developing a clear understanding of the governing physics and incorporating more realistic situations into the model. This approach has generated important analytical developments for specific experimental values of parameters and geometric designs.

Specifically, Kriegsmann & Varatharajah (1993, pp. 382–400) study the heating of a

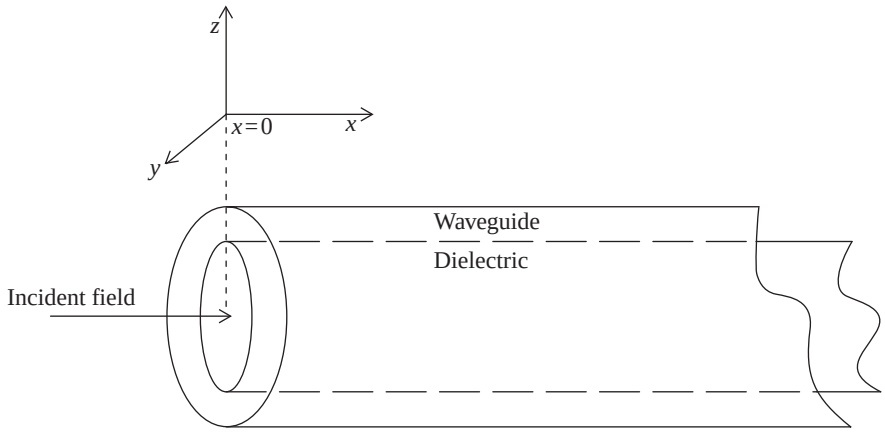

FIG. 1. Travelling wave applicator. A cylindrical dielectric is heated inside a semi-infinite cylindrical waveguide. An incident electric field impinges upon the left boundary of the rod.

thin, ceramic cylinder in a single-mode applicator in the regime of the small Biot number limit. This approximation allows reduction of the original three-dimensional heat equation to a one-dimensional problem and accounts for the loss of heat through the surface. In several of his works, Kriegsmann obtains a heat equation in which the nonlinear term bears a bistable relationship between the power and temperature.

Kriegsmann has also developed a systematic mathematical modelling theory which includes S-matrix theory and a small Biot number asymptotic analysis. His theory has inspired many related studies on microwave heating. His derivations have became standard procedure. Most recently he has expanded his results to include more rigorous studies of certain problems ((1997) and references therein) and also he has continued developing more realistic and complex scenarios from the state of the art microwave heating research including theoretical aspects and practical applications.

Particularly relevant to this paper is the work of García-Reimbert *et al.* (1996). Building on the previous work of Kriegsmann and others, they studied the formation and propagation of hotspots (strictly speaking, temperature fronts in the form of a travelling wave) in a single-mode, coaxially-loaded, cylindrical cavity (travelling wave applicator), in the limit of small thermal diffusivity; see Fig. 1. In their study, García-Reimbert *et al.* assume that a plane wave of high frequency radiation impinges upon the left boundary of a dielectric beginning at time $t = 0$. The left boundary is positioned at the origin. The left end of the cylinder is assumed to be perfectly thermally insulated, so that energy can only be lost due to diffusion from the cylindrical boundary of the rod. They also assume that the cylinder is infinite and the detuning effects and the interactions between the dielectric and the waveguide are ignored. The study takes into account the interaction between the temperature front and a non-uniform electric field. García-Reimbert *et al.* use a WKB approximation to obtain an asymptot of the electric field in the limit of small thermal conductivity.

1.2 *Mathematical model*

The model studied here is the one derived by García-Reimbert *et al.* (1996). The following one-dimensional system describes the evolution thermal fronts in a semi-infinite cylinder with the geometry described above:

$$E_{tt} - E_{xx} + \lambda^2 E + \sigma(T)E_t = 0, \tag{1.1}$$

$$T_t = \nu T_{xx} + \rho f(T, |E|) \tag{1.2}$$

for $x \geqslant 0, t \geqslant 0$. Here, λ represents the characteristic cut-off frequency of the waveguide, σ is the temperature dependent electric conductivity with functional form $\sigma(T) = \sigma_0 + \sigma_1 T$, ν is the thermal diffusivity of the dielectric, and ρ parametrizes the intensity of the electric field (its heating effect on the material). The corresponding initial and boundary conditions are $E(0, t) = e^{iqt}$ and $E(x, 0) = E_t(x, 0) = 0$ for the electric field, and $T_x(0, t) = 0$, $T(x, 0) = 0$ for the temperature field. The parameter q is the frequency of the incident electric field.

The coupling between (1.1) and (1.2) is defined by $f(T, |E|) = (T^2 - T + \gamma|E|)(1 - T)$, where γ and ρ control the rate at which the material takes up heat energy. The coupling functions f and σ determine most of the interesting dynamics observed in the solutions on the system (1.1)–(1.2), so it is of interest to discuss their particular form.

From the earliest works, for example, (Kriegsmann & Varatharajah, 1993), a nonlinear, cubic function was derived to account for the coupling of $|E|$ and the loss of heat through the boundary of a circular cylindrical dielectric. In several of Kriegsman's works, an S-shaped response curve relating the steady-state temperature to the microwave power has been discussed as a possible explanation for the thermal runaway phenomenon responsible for the formation of hotspots.

A convenient innovation of García-Reimbert *et al.* (1996) was to replace the complicated bistable form by a canonical cubic as the one above. The general, cubic, bistable, nonlinear term qualitatively captures the relation between the intensity of the electric field and temperature and the loss of heat through boundaries.

The assumption of a linear relation between electrical conductivity and temperature, as we have adopted here, has become a standard procedure to simplify their dependence, for example, (García-Reimbert *et al.*, 1996; Smyth, 1990). Although experimental evidence suggests that temperature dependence of many materials can be represented by a power law or an exponential, the above assumption should account adequately for weak dependence of σ on temperature.

Although the forms of f and σ for a given application might differ quantitatively or be more complicated, the somewhat tractable mathematical model considered here is sufficiently complex to capture some of the non-trivial nonlinear behaviour that can occur, and hence is useful for seeking new insights into the heating process.

In particular, as in (García-Reimbert *et al.*, 1996), f can be written as

$$f = (T - T_l)(T - T_s)(T_r - T), \tag{1.3}$$

where the roots are given by

$$T_l = 1, \quad T_r = \tfrac{1}{2}\big(1 - \sqrt{1 - 4\gamma|E|}\big), \quad T_s = \tfrac{1}{2}\big(1 + \sqrt{1 - 4\gamma|E|}\big). \tag{1.4}$$

Note that f will have either exactly three real roots or one, depending on the value of $\lambda|E|$. The bistability that results in the case of three real roots leads to the existence of travelling wave behaviour in the temperature field.

In the following, our analysis is primarily restricted to parameter regimes where $\rho \gg 1$, $\nu/\rho \ll 1$, and γ of order one or greater ($\gamma \gg 0$). Fortunately, these regimes are the most physically relevant because in typical industrial microwave heating applications the diffusion of heat (governed by ν) will tend to occur more slowly than the heating due to the high intensities of the applied electric fields (the rate of heating being controlled by ρ). As we remark at relevant places later on, some of our results appear to be useful even when these conditions are not strictly met.

Numerical simulations suggest that the overall dynamics of this model can be characterized by three consecutive evolutionary stages. First, the electric field begins to penetrate the material and there is rapid formation of a temperature front (the 'formation' stage). Secondly, this temperature front propagates into the material in concert with the electric field (the 'transient' stage). Thirdly, the fields relax to a steady-state configuration (the 'steady-state' stage).

The questions we attempt to answer in this paper for the model above are as follows. (1) What are the profiles of the electric field and the temperature front during the transient and steady-state stages? (2) What are the temporal dynamics of the transient stage? (3) What is the penetration depth of the fields at the final steady state?

The rest of the paper is organized as follows. In Section 2, we develop an approximation to equation (1.2), in the limit of small diffusivity, called the *free boundary problem* (FBP), which partially solves the model (1.1)–(1.2), yielding information about the temperature field profile and its coupling to the electric field. In particular, the asymptotic temperature field is found to take the form of a front whose dynamics (location vs. time) depend on the magnitude of the electric field. The location of this front is the so-called 'free boundary'. Although this procedure has been used to study hyperbolic systems, it is the first time, to our knowledge, that it has been successfully applied to microwave related problems with mixed systems of parabolic and hyperbolic nature.

In Section 3, we combine the FBP results with a time harmonic approximation of the electric field to obtain equations for the steady state which can be solved in closed form when a reasonable approximation for the temperature is made. The resulting solution generalizes those found before in related studies, and we verify its usefulness numerically.

Finally, we analyse the transient dynamics prior to steady state by means of a quasi-stationary-state approximation that well describes the dynamics of the position of the temperature front and the relaxation of the electric field into the dielectric. We also present numerical comparisons for these results.

2. Free boundary problem

As we will now show, when the ratio ν/ρ is small and ρ is large, the asymptotic dynamics of the temperature profile can be characterized as a sharp temperature front that propagates inside the cylinder. The propagation of the front depends in detail on the behaviour of the electric field, which we analyse in the next two sections. Although these fronts are not strictly travelling waves, because they do not propagate at a constant speed for all

time, the procedure adopted here resembles those widely used to study travelling waves in hyperbolic systems.

Based on the numerical observation that the electric field amplitude generally remains monotonically decreasing in x as the field moves into the material, we assume at the outset that this is always the case. At points x of the space domain where $|E(x,t)| > 1/4\gamma$, that is, positions in the material between $x = 0$ and the point at which $|E|$ has decreased to $1/4\gamma$, the cubic function $f(T,|E|)$ (equation (1.3)) has only one root ($T_l = 1$) with negative slope with respect to T at this point. Moreover, at the first stages of the formation of the front, the values of temperature are small such that $\rho f \gg 1$ such that the diffusion term can be neglected. Therefore, the evolution of the temperature field in mainly dictated by the equation $T_t = \rho f$ and temperature evolves towards one quickly. As T approaches closely to one its evolution slows, and it relaxes arbitrarily slowly. Once the front has formed, in the subregion of this domain which is not too close to the temperature front, that is, in regions where the diffusion term can be neglected, the evolution of the temperature field still is being controlled mainly by the ODE $T_t = \rho f(T,|E|)$, and the temperature at all points in this subregion will monotonically increase with time and asymptotically approach the value one ($T \to T_l = 1$). This behaviour partially explains the rapid formation of the temperature front and its slow motion after formation.

Likewise, for points where $|E(x,t)| < 1/4\gamma$, the cubic function $f(T,|E|)$ has three roots, and it is straightforward to show that, away from the temperature front diffusion can again be neglected, and the temperature in this region approximately approaches the stable root $T_r = \frac{1}{2}\big(1-\sqrt{1-4\gamma|E|}\big)$ (and slightly overshoots due to a small diffusive correction). Note that this root depends pointwise on the value of E, thus slaving part of the temperature profile to E.

So far, these considerations suggest that the temperature profile will tend to assume the shape of a front with the form

$$T(x,t) = T_l \cdot \chi_{[0,x_s]} + T_r(|E|) \cdot \chi_{[x_s,\infty)}, \tag{2.5}$$

where the characteristic functions $\chi_{[0,x_s]}$ and $\chi_{[x_s,\infty)}$ allow us to combine the two separate profiles into one expression. In these expressions, the position $x = x_s$ represents the location of the front, which will presumably lie close to the point at which $|E(x,t)| = 1/4\gamma$ (we confirm this below).

It thus remains to determine the *dynamics* of x_s in response to the electric field profile $E(x,t)$. At the point x, where $|E(x,t)| = 1/4\gamma$, the coupling term f has a double root, $T = \frac{1}{2}$. The dynamics of the temperature here will be more complicated. In particular, the diffusion term can no longer be neglected in at least a region $\Delta x = \nu/\rho$.

Following Fife (1988), we can make progress in determining the motion of the temperature front by invoking the so-called *free boundary problem* reduction, the results of which only we will restate here. The reduction proceeds as follows.

Based on the fact that $\rho \gg 1$ and $\nu/\rho \ll 1$, we for the moment suppose that $|E(x,t)|$ is fixed in time (take a 'snapshot' of E at some moment; $E(x,t) \to E(x)$) and sufficiently smooth in space. We then construct an approximate solution for the heat equation using the method of matched asymptotic expansions. The outer solutions are found using a regular expansion, and the inner solutions by front layer expansion under the additional scaling assumption $\rho = O(1/\nu)$ (which is more specific but not inconsistent with our general assumption that $\nu/\rho \ll 1$).

Using the results from this procedure, and restoring slow time dependence to E, we find that, to order $O(1/\nu)$ in time, the system consisting of equations (1.2) and (1.1), the full system to the *free boundary problem*

$$E_{tt} - E_{xx} + \lambda^2 E + \sigma(T)E_t = 0, \tag{2.6}$$

$$T(x,t) = T_l \cdot \chi_{[0,x_s]} + T_r(|E|) \cdot \chi_{[x_s,\infty)}, \tag{2.7}$$

$$\dot{x}_s(t) = \tfrac{1}{2}\sqrt{\tfrac{1}{2}\rho\nu}\left(1 - 3\sqrt{1 - 4\gamma|E(x_s(t))|}\right), \tag{2.8}$$

with the boundary conditions $E(0,t) = \mathrm{e}^{\mathrm{i}qt}$ and $E(x,0) = E_t(x,0) = E(\infty,t) = 0$ for the electric field.

Note that the dynamics of the front position $x_s(t)$ are now governed by the ordinary differential equation (2.8) which depends parametrically on $|E(x,t)|$ evaluated at $x = x_s(t)$. In particular, we have $\dot{x}_s(t) = 0$ for $x_s = X_s$ such that $E|(X_s)| = 2/9\gamma$, which implicitly determines the steady-state location for the temperature front (this point is unique if $E(x,t)$ is monotonically decreasing in x). Examination of (2.8) shows that the steady-state condition $\dot{x}_s = 0$ is always asymptotically approached for a fixed and monotonically decreasing electric field profile.

Note further that the speed $\dot{x}_s$ can only take values between 0 and $\frac{1}{2}\sqrt{\frac{1}{2}\rho\nu}$ in the FBP system. The latter value is implicitly defined by $|E(x_s)| = 1/4\gamma$, which is the value at which the coupling function f first attains three roots. This occurs at the onset of validity of the FBP and represents the maximum speed within the validity of the FBP. This illustrates the important point that the FBP is valid only well after the temperature front has formed.

Although the dynamics of this process happen on a relatively slow time scale, the evolutionary stage represented by the FBP fortunately contains most of the interesting dynamics involving interactions between the electric and temperature fields, which occur when the reaction term ρf approximately counterbalances the temperature diffusion term. In all of these respects the situation is similar to the fast interface asymptotic reduction of FitzHugh–Nagumo systems in (Fife, 1988). Also see (Chen, 1992) for a more rigorous justification.

Note that in the FBP reduction, both the temperature profile and the location of the temperature front are now both *slaved* to the electric field. In this way, the original problem has been substantially reduced—if we can also provide a way to analyse the dynamics of the electric field as a function of this reduced temperature field, then we can in principle eliminate the temperature field using the FBP and thereby solve the entire system. This is what is undertaken in the next two sections for the steady-state and transient regimes, respectively.

Obviously, the complexity involved in solving for E with T eliminated in this way will depend crucially on the how the temperature field in turn affects the behaviour of the electric field. This nature and strength of this coupling and the behaviour of E is controlled by the relative values of σ_0 and σ_1. In particular, the value of σ_1 tunes the effect of temperature on equation (2.6). When its value is small, E is largely independent of T. On the other hand, σ_0 determines a rate of decay of $|E|$ which is independent of temperature. As a result, we refer to σ_0 as the absolute electric conductivity and σ_1 as the relative electric conductivity. A regime in which σ_1/σ_0 is small may be referred to as one of weak coupling of E with temperature and strong absolute decay. On the other hand, when σ_1/σ_0 is large,

the decay of E will be largely controlled by temperature. In this case, temperature and electric fields are both strongly coupled to one another.

To conclude our observations about the free boundary problem reduction, we point out that when ν/ρ is small, the temperature profile is well described by equation (2.7) and takes the form of a sharp front, the movement of which is well described by equation (2.8). On the other hand, when ν/ρ is not small, the actual temperature profile smoothes out in contrast to the asymptotic solution (2.7). We remark, however, that in many of our numerical experiments in this latter regime we have found that the location of the temperature front at steady state still seems to be quite accurately described by equating (2.8) to zero. This is probably due to an averaging effect, the lowering of temperature to the left of X_s being balanced to a significant extent by the raising of T to the right of X_s.

3. Steady-state solutions

As stated above, numerical simulations suggest that the solution of equations (1.1), (1.2) asymptotically tend to a steady state in which the electric field intensity and temperature profiles are temporally constant and the electric field phase oscillates harmonically with radian frequency q. This is reasonable physically, and represents an asymptotic balance between a constant energy input and the heat losses due to radiation and convection. Note, however, that its occurrence is not a priori obvious due to the strong nonlinearities present in the system.

In the previous section we have shown how the FBP provides a reduced description for the dependence of the temperature on electric field in the limit of low thermal diffusivity relative to heating rate. Although equations (2.6)–(2.8) of the FBP retain the nonlinear character of the original system, they are more tractable, in particular for the study of steady-state solutions. For instance, setting $\dot{x}_s = 0$ in equation (2.8), yields the condition $|E(X_s)| = 2/9\gamma$, where X_s denotes the final position of the temperature front. This equation implicitly determines the final position of the temperature front in terms of the intensity of the electric field.

We now seek an analytical approximation of the steady state to provide us with a prediction for the profile of the electric field. In simulations, for sufficiently large time, the intensity profile of the electric field is observed to become constant. We therefore make the following harmonic ansatz:

$$E(x, t) = A(x)\mathrm{e}^{\mathrm{i}qt}.$$

Here A is a complex-valued function (the true value of the electric field being obtained by taking the real part of the expression above). Inserting this approximation into equation (2.6), and setting $\dot{x}(t) = 0$ in equation (2.8), we obtain the steady-state equations for the free boundary problem:

$$A_{xx} + \omega^2(T)A = 0, \tag{3.9}$$

$$T(x; X_s) = T_l \cdot \chi_{[0,X_s]} + T_r(|A|) \cdot \chi_{[X_s,\infty)}, \tag{3.10}$$

$$|A(X_s)| = \frac{2}{9\gamma}, \tag{3.11}$$

where $\omega^2(T) = q^2 - \lambda^2 - \mathrm{i}q\sigma(T)$, $\sigma(T)$, T_l and T_r are as defined previously. Notice that the resulting system is still difficult to solve due to the nonlinear coupling between A and T through the functions $\omega^2 = \omega^2(T)$ and $T_r = T_r(|A|)$.

To make progress, we exploit the following idea. If γ is not too small, say of order one or greater, then condition (3.11) implies that the point X_s at which the temperature front is located will occur at a point at which the electric field is much less than 1 (one being the maximum strength of the field at $x = 0$). More specifically, if $\gamma > 1$, then X_s must lie beyond the point at which $|A| = 2/9\gamma|_{\gamma=1} = 0{\cdot}\overline{22}$. Therefore, for large γ, most of the influence of temperature on the electric field should occur to the left of the temperature front, where $T = T_l = 1$.

To strengthen this argument, we further observe that for electric field profiles which approximately take the form of a decaying exponential, which, as we discuss later, is always true if either $\sigma_1/\sigma_0 \ll 1$ or γ is not too small, then the *form* of the temperature function $T = T_r(|E|) = \frac{1}{2}\big(1 - \sqrt{1 - 4\gamma|E|}\big)$ becomes independent of γ. Specifically, if $|E|$ has the form $|E| = \mathrm{e}^{-\alpha x}$, then condition (3.11) implies that $X_s = -(1/b)\ln(2/9\gamma)$. Defining a new space variable $\tilde{x}$, such that $\tilde{x} = x - X_s$, using this to eliminate x in $|E| = \mathrm{e}^{-\alpha x}$, and inserting the resulting expression into $T_r(|E|)$, we find that $T_r(|E|) = \frac{1}{2}\big(1 - \sqrt{1 - \frac{8}{9}\mathrm{e}^{-b\tilde{x}}}\big)$, that is, $T_r(|E|)$ is independent of γ aside from the location X_s. If follows from this that increasing γ with other parameters fixed simply shifts the temperature profile to the right without appreciably altering its form. Given the approximately exponential form of the electric field, this implies that increasing γ will exponentially decrease the effect of the temperature to the right of the front.

Thus, if γ is not too small, we should be able to approximate T in equation (2.7) by setting $T_r = 0$, without significantly affecting the intensity profile of E. This range should include regimes where σ_0 and σ_1 are significantly greater than 1. In this way, T_l becomes a piecewise constant approximation for T with a single discontinuity at $x = X_s$. Numerical experiments, including those given later in this section, seem to confirm that this leads to accurate predictions for $q \gg 0$. This idea may also be applied to the dynamics of the transient regime, which we discuss in the next section.

Besides the considerations just described, the reason that this approximation works for γ of order one and greater, instead of only for much larger values of γ, also appears to be in part a consequence of the fact that T_r is less than $0{\cdot}\overline{33}$ everywhere to begin with, and decreases exponentially fast in x if $|E|$ does also. This implies that T_r can have a significant influence on E relative to $T_l = 1$ only for values of γ on the order of $\gamma = \frac{9}{2}$, that is, the values for which X_s is approximately zero.

We now obtain solutions of (3.9)–(3.11), with the approximation $T_r = 0$, in a closed form expression for the intensity profile of the electric field at the steady state. Its more complicated form precludes the possibility of obtaining an explicit solution for the location of the temperature front, except in certain limits. The closed form expression for the magnitude of the electric field, however, is valid for a wide range of values of parameters.

Imposing the boundary conditions $A(0) = 1$ and $A(\infty) = 0$ and the approximation $T_r = 0$ on equations (3.9)–(3.11), an exact solution is obtained by first solving the ordinary differential equation at both sides of the temperature front separately and applying

matching conditions up to the first derivative. This results in the unique C^1 solution

$$A(x;\, X_s) = \begin{cases} K2\mathrm{i}\sin(\omega_f x) + \mathrm{e}^{-\mathrm{i}\omega_f x}, & x \leqslant X_s, \\ \left[K2\mathrm{i}\sin(\omega_f X_s)\mathrm{e}^{\mathrm{i}\omega X_s} + \mathrm{e}^{\mathrm{i}(\omega-\omega_f)X_s}\right]\mathrm{e}^{-\mathrm{i}\omega x}, & x \geqslant X_s. \end{cases} \tag{3.12}$$

where

$$K = K(X_s;\, \omega_f, \omega) = \frac{\omega_f - \omega}{(\omega_f - \omega) + (\omega_f + \omega)\mathrm{e}^{2\mathrm{i}\omega X_s}}. \tag{3.13}$$

The values of ω, b and a are given by $\omega = a - \mathrm{i}b$, $a = q\sigma_0/2b$ and $b = \sqrt{\frac{1}{2}\left\{|\omega^2| - (q^2 - \lambda^2)\right\}}$ and represent the values of ω and σ evaluated to the right of X_s, where T is approximated as $T = 0$, and hence $\sigma(T) = \sigma_0$. The values of ω with the subscript f added represent the values evaluated on the left-hand side, where $T = T_l = 1$ and hence $\sigma(T) = \sigma_0 + \sigma_1$, and are given by $\omega_f^2 = (q^2 - \lambda^2) - \mathrm{i}q(\sigma_0 + \sigma_1)$, $\omega_f = a_f - \mathrm{i}b_f$, $a_f = q(\sigma_0 + \sigma_1)/2b$ and $b_f = \sqrt{\frac{1}{2}\left\{\left|\omega_f^2\right| - (q^2 - \lambda^2)\right\}}$ (note that these two different sets of values are mixed in the expressions above by the solution matching at $x = X_s$).

The position of the front at the steady state is then uniquely determined by the implicit function theorem applied to condition (3.11) evaluated on (3.12) for *any* general choices of the parameters σ_0 and σ_1. The value of X_s can very easily be determined numerically in this way, and this approach to finding X_s therefore generalizes the results of García-Reimbert *et al.* (1996), which are based on low conductivity ($\sigma_1, \sigma_0 \ll 1$).

Another approach to finding X_s in the limit of small σ_1 (weak dependence of the electric field on temperature), using the same approximation $T_r = 0$ as before, is to perform a regular asymptotic expansion for the solution of system (3.9)–(3.11), with $T_r = 0$. This results in easier expressions for obtaining information about X_s in the limit of small σ_1 (with σ_0 still possibly large, allowing for strong decay of the electric field in x), or closed form expressions for X_s in the limit of small σ_0 and σ_1.

Applying this regular asymptotic procedure through second order in σ_1, we obtain the following $C^1(R^+)$ solution, along with a solvability condition $2\mathrm{i}\mathrm{e}^{-2\mathrm{i}\omega X_s} \neq 0$ which is always satisfied,

$$\begin{aligned} A(x;\, X_s) &= A_0(x;\, X_s) + \sigma_1 A_1(x;\, X_s) + O(\sigma_1^2) \\ &\simeq \begin{cases} \left[1 + \dfrac{\mathrm{i}q}{4\omega^2}\mathrm{e}^{-2\mathrm{i}\omega(X_s)}(1 - \mathrm{e}^{-2\mathrm{i}\omega x}) - \dfrac{q}{2\omega}x\right]\mathrm{e}^{-\mathrm{i}\omega x}, & x \leqslant X_s, \\ \left[1 + \dfrac{\mathrm{i}q}{4\omega^2}\mathrm{e}^{-2\mathrm{i}\omega(X_s)}(1 - \mathrm{e}^{2\mathrm{i}\omega(X_s)}) - \dfrac{q}{2\omega}X_s\right]\mathrm{e}^{-\mathrm{i}\omega x}, & x \geqslant X_s. \end{cases} \end{aligned} \tag{3.14}$$

As stated above, this equation can easily be used to obtain results for small σ_1. For example, setting $x = X_s$ and for $\sigma_0, \sigma_1 \ll 1$, equation (3.14) becomes

$$A(X_s;\, X_s) = \left[1 - \sigma_1\frac{\mathrm{i}q}{4\omega^2}(1 - \mathrm{e}^{-2\mathrm{i}\omega(X_s)}) - \frac{q}{2\omega}\sigma_1 X_s\right]\mathrm{e}^{-\mathrm{i}\omega X_s} + O(\sigma_1^2).$$

In particular when $\sigma_0 \simeq \sigma_1$ are both small we have that this equation can be reduced to

$$|A(X_s;\, X_s)| \simeq \mathrm{e}^{-bX_s}\exp\left\{-\frac{q\sigma_1}{2(a^2 + b^2)}X_s\right\}. \tag{3.15}$$

Expansion of the parameter b also leads to $b \simeq \sigma_0/2\beta$ to leading order in σ_1, where $\beta^2 = (q^2 - \lambda^2)/q^2$, and also $a = q\beta \simeq O(1)$. Inserting these into the coefficient in the exponent of $|A(X_s)|$ we obtain $b + q\sigma_1 a/2(a^2 + b^2) \simeq (\sigma_0 + \sigma_1)/2\beta$. Thus, the last equation can be rewritten as

$$|A(X_s; X_s)| \simeq \exp\left\{-\frac{\sigma_0 + \sigma_1}{2\beta} X_s\right\},$$

which is identical to the result obtained by García-Reimbert *et al.* (1996) in the limit of small σ_0 and σ_1. Our result is therefore consistent with their WKB-approximation. Moreover, equation (3) together with condition (3.11) determine the penetration depth of the temperature profile:

$$X_s \simeq -\frac{2\beta}{\sigma_0 + \sigma_1} \ln \frac{2}{9\gamma}. \tag{3.16}$$

As noted in (García-Reimbert *et al.*, 1996), this approximation works well when σ_0 and σ_1 are small but it breaks down away from this regime. For more general values, using solution (3.12) (for general values of both σ_0 and σ_1) and (3.14) (for small σ_1) can provide us with accurate predictions.

We now compare these analytical results with numerical simulations of the complete system (1.1)–(1.2). The equation for the electric field was numerically solved by a stable, second-order central difference scheme. For the heat equation, a predictor Adams–Bashforth scheme was used. These simulations were numerically coupled by updating each solution of the functions based on the current value of the other variable at each half of each time step.

For all simulations in this paper, the parameters γ and q were fixed at $\gamma = 1$, $q = 2$. We used small values for both ν/ρ, ν, and a large value of ρ to guarantee the validity of the free boundary problem approximation, fixing $\nu = 0{\cdot}01$ and $\rho = 1/\nu$. We then explored the several distinct regimes remaining governed by the relative sizes of the dimensionless parameters σ_0 and σ_1.

Before describing the numerical results, we first briefly comment on some predictions for these different regimes based on the results given above. First, when the quantity σ_1/σ_0 is small, the electric field is largely decoupled from the temperature, and its steady-state amplitude profile should approximate a simple exponential. This can be seen easily from the solution (3.12), by first observing that when $\sigma_1 \to 0$, then $\omega_f \to \omega$, so that $K(X_s; \omega_f, \omega) \to 0$, which leads to $|A| \to \mathrm{e}^{-bx}$. On the other hand, when σ_1/σ_0 is not small, the profile of E will be strongly influenced by the temperature profile, but it will still be *approximately* exponential if X_s is located where $|E|$ is small, that is, if γ is order one or larger (this follows easily from consideration of the solution of the differential equation (3.9) with a constant temperature profile). In either case, if $\sigma_1 + \sigma_0$ is small, then the WKB results of García-Reimbert *et al.*, which predict a piecewise solution with a transition at $x = X_s$, should coincide well with the profile predicted by solution (3.12) or (3.14). We find this to be true, and we omit the numerical demonstrations of this agreement for these regimes here (we remark though that the solution (3.12) reproduces the García-Reimbert *et al.* WKB profile as well, in addition to equation (3.16) accurately predicting the penetration depth). On the other hand, if $\sigma_1 + \sigma_0$ is not small, then we expect either

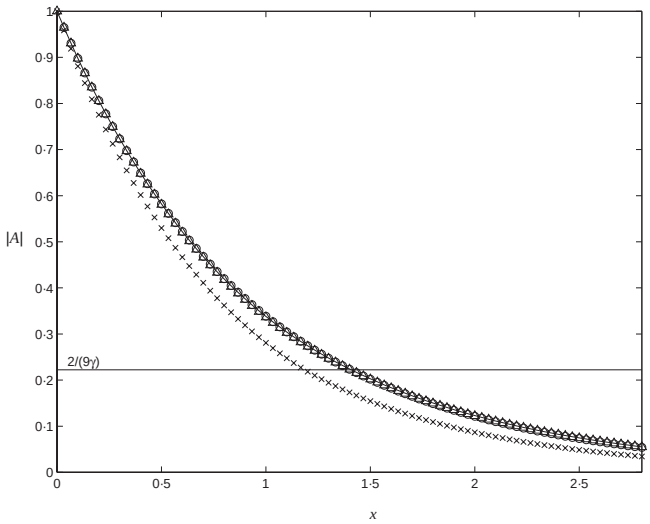

FIG. 2. Steady-state solution of the magnitude of the electric field in the regime of weak temperature dependence and high absolute electric conductivity with values of parameters of $q = 2$, $\gamma = 1$, $\sigma_0 = 2$, $\sigma_1 = 0{\cdot}2$, $\nu = 0{\cdot}01$ and $\rho = 1/\nu = 100$. Circles correspond to the numerical results for system (1.1) and (1.2); the solid curve to the solution given by equation (3.12); triangles to the asymptotic matching (3.14) and crosses represent the profile given by (García-Reimbert *et al.*, 1996, equation 3.20).

the simple exponential case as described above (if σ_1/σ_0 is small), or a more nontrivial solution as predicted by equation (3.12) with nonnegligible value of $K(X_s; \omega_f, \omega)$. In either of these regimes, we expect the profile of E to differ markedly from the WKB results of García-Reimbert *et al*.

The two numerical examples we now describe compare the electric field profiles as given by the steady-state solutions (3.12) and (3.14) with the one found by García-Reimbert *et al.* (1996). In following two figures, circles indicate the profile of the numerical steady-state profile of E for the full system, solid curve represents the profile predicted solution (3.12), crosses show the WKB results of García-Reimbert *et al.* (1996), and triangles represents the asymptotic solution given by formula (3.14).

Figure 2 shows the results obtained by choosing $\sigma_0 = 2$, $\sigma_1 = 0{\cdot}2$, such that $\sigma_1 + \sigma_0$ is not small but σ_1/σ_0 is, representing a regime with large absolute electric conductivity and weak coupling to temperature. As expected, we find good agreement between the numerical profile and solution (3.12) and also the asymptotic matching solution (3.14) (the latter because σ_1 is small), and significant disagreement with the WKB profile of García-Reimbert *et al*.

Figure 3 shows the results obtained by choosing $\sigma_0 = 2$, $\sigma_1 = 2$, such that neither $\sigma_1 + \sigma_0$ nor σ_1/σ_0 is small, representing a regime with large absolute electric conductivity and strong coupling to temperature. As expected, we find good agreement between the numerical profile and solution (3.12), and significant disagreement between these and the asymptotic matching solution (3.14) and also the WKB profile of García-Reimbert *et al*.

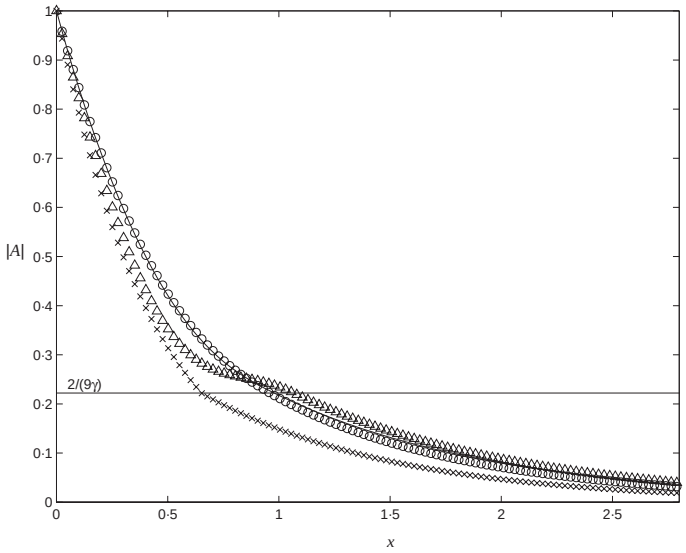

FIG. 3. Steady-state solution of the magnitude of the electric field for the regime with strong temperature dependence and high absolute electric conductivity. Values of parameters and lines are same as in Fig. 2, except $\sigma_1 = 2$.

To conclude the comparison, we remark that other numerical experiments suggest that the analytical results found above appear to work well in describing electric field profiles for values of ν as great as 0·6 with $\rho = 1/\nu$. On the other hand, even though the *location* of the temperature front is still well predicted by equation (2.7), the prediction of its profile largely disagrees for $\nu \gg 1$.

4. Transient solutions

In this section, we study the time evolution of the temperature and electric field fronts as they relax to their respective steady states. We use a quasi steady-state approximation for the electric field similar to the time harmonic steady-state solutions studied in the previous section.

In Section 2 the relaxation of the temperature field to a steady-state profile in the presence of a *fixed* electric field was studied. Recall that this process was shown to occur in two stages. First, the temperature front forms on a fast time scale of order $1/\rho$, at points x in a subregion of the domain such that $|E(x,t)| > 1/4\gamma$, where the reaction term has only a single root, $T = 1$.

Secondly, when the temperature front has advanced to a point such that this inequality is not satisfied, then the reaction term becomes bistable, and the temperature front attempts to relax more gradually to a steady-state with position X_s defined implicitly by $|E(X_s^T)| = 2/(9\gamma)$ (that is, when the free boundary problem analysis is valid).

The free boundary analysis assumes that the electric field is either stationary or evolves on a very slow time scale relative to the temperature front. Note that if γ is large, then the

width of interval I in x,

$$\frac{2}{9\gamma} \leqslant |E(x)| \leqslant \frac{1}{4\gamma}, \tag{4.17}$$

will be small. In order for the free boundary problem to correctly describe the temperature front, the front's position x_s must lie in this interval.

We observe that if the time scale of the temperature front evolution, which is of order $1/\rho$, is faster than the one at which the *electric field* front propagates, then the temperature front should closely follow the electric field front, that is, the temperature front will be 'slaved' to the electric field as it relaxes, *except for a small lag on the order of the interval* I. We confirm later that this will be the case if $1/\rho \ll 1/(\sigma_0 + \sigma_1)$.

To analyse the propagation of the electric field for situations when this slaving is fulfilled through the transient stage, we now make a quasi-steady-state ansatz for the electric field.

This ansatz is based in part on numerical observations that the electric field apparently relaxes to its steady-state profile by the gradual propagation of a fairly steep front into the material, such that, as it propagates, the field appears to gradually fill out its steady-state profile as it goes (or more precisely, a series of these profiles, each roughly consistent with the instantaneous position of the temperature front). This is not to say that the whole field profile resembles a steady-state profile at each instant; rather, that the electric field appears to exhibit a steady-state-like profile *behind* its steeply sloped and advancing front edge.

Assuming that such a front exists during the transient stage, and has a monotonically decreasing amplitude at all times, we now *define* the position of the electric field front to be the instantaneous and unique point $x = x_s^E$ at which $|E(x_s^E)| = 2/9\gamma$. Note that this definition is identical to the implicit steady-state equation for the temperature front derived from the FBP. Assuming that the temperature front, the position of which we represent here by x_s^T, is 'slaved' to the electric field profile at each instant, then this definition implies that $x_s^T \approx x_s^E$.

We next make the following ansatz for the electric field:

$$E(x,t) = \begin{cases} A(x; x_s^E(t))\mathrm{e}^{\mathrm{i}qt}, & x \leqslant x_s^E(t), \\ 0, & x > x_s^E(t). \end{cases} \tag{4.18}$$

Here, the functions $A(x;\delta)$ represent the one-parameter family of steady-state electric field profiles that would be obtained by allowing the electric field to attain a steady-state profile in the presence of *fixed* temperature fronts at locations $X_s^T = \delta$, that is, the ansatz (4.18) incorporates the temperature fields *parametrically*. By equation (3.9), the family $A(x;\delta)$ solve the equation $A_{xx} - \omega(T)A = 0$, with a fixed temperature front located at $X_s^T = \delta$. As in the previous section, we assume that these temperature fronts can be effectively modelled as

$$T = \begin{cases} 1, & x \leqslant \delta, \\ 0, & x \geqslant \delta. \end{cases} \tag{4.19}$$

The ansatz also imposes the approximation that the electric field vanishes for $x > \delta$, in accordance with the numerical observations that the electric field front is generally very

steep. Note that this assumption automatically solves the Maxwell equation in this region trivially. It then remains to enforce the Maxwell equation on the interval $[0, x_s^E]$.

Inserting (4.18) into (2.6) leads to the equation

$$A'\dot{x}_s^{E2} + A'(\ddot{x}_s^E - 2\mathrm{i}q\dot{x}_s^E + \sigma(T)\dot{x}_s^E) = (A_{xx} - (\lambda^2 - q^2 - \mathrm{i}q\sigma(T))A), \tag{4.20}$$

where a prime means $\partial/\partial\delta$ (note that this is not a *spatial* derivative, but this appears because $x_s^E(t)$ is a time dependent parameter in the ansatz), and where an over-dot is a time derivative. Dividing by A' (assuming it is not zero, which is justified below) and taking real and imaginary parts, we have

$$\ddot{x}_s^E(t) + \sigma(T)\dot{x}_s^E + \mathrm{Re}\left(\frac{A''}{A'}\right)\dot{x}_s^{E2} = \mathrm{Re}\left[\frac{A_{xx} - (\lambda^2 - q^2 - \mathrm{i}q\sigma(T))A}{A'}\right],$$

$$-2q\dot{x}_s^E + \mathrm{Im}\left(\frac{A''}{A'}\right)\dot{x}_s^{E2} = \mathrm{Im}\left[\frac{A_{xx} - (\lambda^2 - q^2 - \mathrm{i}q\sigma(T))A}{A'}\right].$$

The right-hand sides of these equations vanish identically, because A solves the equation in the numerators, which is simply the equation for the steady-state profile (equation (3.9)). The second equation is trivially solved by $\dot{x}_s^E = 0$, which is a good approximation as steady state is approached, and we henceforth neglect this equation.

With the vanishing of the right-hand side, the first equation reduces to

$$\ddot{x}_s^E(t) + \sigma(T)\dot{x}_s^E + \mathrm{Re}\left(\frac{A''}{A'}\right)\dot{x}_s^{E2} = 0. \tag{4.21}$$

We will demonstrate that equation (4.21) is quite useful for describing the relaxation of the electric field. Because this equation describes the enforcement of the Maxwell equation in the interval $[0, x_s^E]$, where $T = 1$ by (4.19), we will consistently approximate the value of σ in equation (4.21) by $\sigma(T = 1) = \sigma_0 + \sigma_1 \equiv \Sigma$.

Note that the coefficient A''/A' of the nonlinear term depends *a priori* on x. To properly enforce the Maxwell equation, this x dependence must drop out (it does, as we show below).

To approximate A''/A', we will take advantage of expressions (3.12) and (3.14), which are the expressions for the steady-state consistent with (4.19). We will now use these expressions, however, with the parameter X_s made variable and set equal to $\delta = x_s^E$. We shall find that expressions (3.14) give a constant value for A''/A'—in the limit of small σ_1—allowing equation (4.21) to be solved exactly. Equation (3.12) will lead to a nonlinear ordinary differential equation for x_s^E which works well in all regimes, but which must be solved numerically.

In the limit of small σ_1, we use expression (3.14) to approximate the coefficient A''/A' in the following way. Differentiating (3.14) with respect to X_s, we obtain

$$\frac{\partial A}{\partial X_s} = \frac{q}{2\omega}\mathrm{e}^{-\mathrm{i}\omega(x+2X_s)}, \tag{4.22}$$

$$\frac{\partial^2 A}{\partial {X_s}^2} = -\mathrm{i}q\mathrm{e}^{-\mathrm{i}\omega(x+2X_s)}, \tag{4.23}$$

and hence

$$\mathrm{Re}\left(\frac{A''}{A'}\right) \simeq \mathrm{Re}(-\mathrm{i}2\omega) = \mathrm{Re}(-\mathrm{i}2(a - \mathrm{i}b)) = -2b. \tag{4.24}$$

Thus, the x dependence has dropped out, as foreshadowed above. With this expression for $\mathrm{Re}(A''/A')$, equation (4.21) becomes a second-order (nonlinear) ordinary differential equation with constant coefficients. With the vanishing of the right-hand side, the first equation reduces to

$$\ddot{x}_s^E(t) + \sigma(T)\dot{x}_s^E - 2b\dot{x}_s^{E2} = 0. \tag{4.25}$$

This must be solved subject to the boundary conditions

$$x_s^E(t = 0) = 0, \quad \lim_{t\to\infty} x_s^E(t) = X_s^T, \tag{4.26}$$

where X_s^T is the asymptotic position of the temperature front as calculated from either condition (3.11) or (3.16) (the former being used if σ_1 is not small). The (unique) solution is given by

$$x_s^E(t) = \frac{1}{B}\log\left[1 - (1 - \mathrm{e}^{-BX_s^T})\mathrm{e}^{-\Sigma t}\right] + X_s^T, \tag{4.27}$$

where $B = -2b$. Equation (4.27) describes an increasing monotonic function with respect to time with the asymptotic value $x = X_s^T$ as $t \to \infty$. As the examples below will show, this function quite accurately describes the front propagation obtained by numerical integration of the full system (1.1)–(1.2) when σ_1 is small.

To analyse the more general case, that is, when σ_1 is not small, we first point out that for equation (3.12), we have $\mathrm{Re}(A''/A') = \mathrm{Re}(K''/K')$, where $K = K(X_s; \omega_f, \omega)$ is defined by (3.13). Thus, the x dependence drops out in the more general case as well, although the value is not a constant with respect to x_s^E in this case, precluding a closed form solution of equation (4.21).

Computing the following derivatives, $\partial K/\partial X_s$ and $\partial^2 K/\partial X_s^2$, we obtain

$$\mathrm{Re}\left(\frac{A''}{A'}\right) \simeq \mathrm{Re}\left\{2\mathrm{i}\omega\left[1 - \frac{2(\omega_f - \omega)}{(\omega_f - \omega)\mathrm{e}^{-2\mathrm{i}\omega_f X_s} + (\omega_f + \omega)}\right]\right\}. \tag{4.28}$$

It can be shown that this expression reduces to equation (4.24) in the limit $\sigma_1 \to 0$. Equation (4.21) can be integrated numerically with this expression inserted to obtain a prediction of the relaxation of E. We remark that we have found it worthwhile to simply substitute the asymptotic value of this expression for B in closed form solution (4.27). This apparently works well due to the oscillatory behaviour in equation (4.28) which averages out the effect of the x_s^E dependence in this term.

As in the previous section, we now illustrate some of the analytical results obtained above by presenting simulations with several sets of parameters corresponding to qualitatively distinct regimes. As before, we take $q = 2$, $\gamma = 1$, $\nu = 0{\cdot}01$ and $\rho = 1/\nu = 100$. The distinct behaviour in each regime is thus governed by the relative sizes of the dimensionless parameters σ_0 and σ_1.

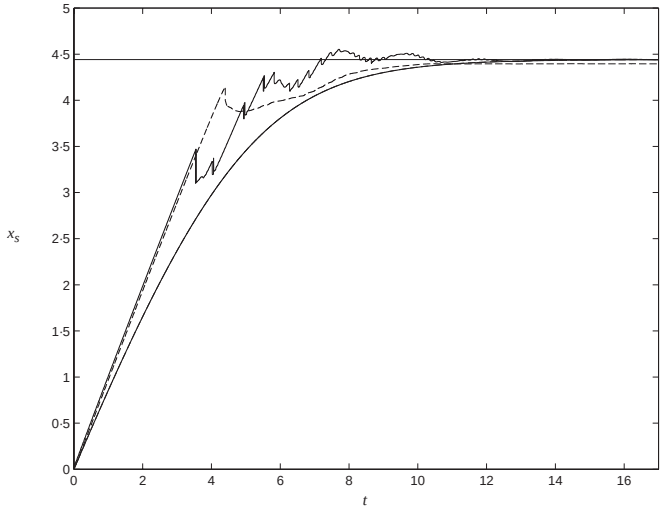

FIG. 4. Comparison of the numerical and analytical results for the relaxation of the electric and temperature fields to steady-state ($\sigma_0 = 0{\cdot}5$, $\sigma_1 = 0{\cdot}1$); weak-temperature dependence and small absolute electric conductivity. The solid curve with high order oscillations corresponds to the time evolution of the electric field front (x_s^E); the dashed curve to the temperature front (x_s^T) and the smooth solid curve represents the values given by equation (4.27). The solid horizontal line represents the final steady-state position of the electric and temperature fronts.

Figures 4 and 5 illustrate the process of relaxation to the steady state of the field fronts, respectively. The figures show the numerically obtained front propagation curves (solid curves with high oscillations—electric field front, dashed curves—temperature front), which are computed from numerical simulations of the complete system (1.1)–(1.2). The front positions were obtained at each time step using the criteria $T(x_s^T, t) = \frac{1}{2}T(0, t)$ and $|E(x_s^E(t))| = 2/9\gamma$, which are consistent with the foregoing analysis (the former arises from the inner expansion associated with the FBP analysis).

First, we note first that condition $1/\rho \ll 1/(\sigma_0 + \sigma_1)$ is well met for both examples. On this basis we predict that the temperature front will be strongly slaved to the electric field front and that, hopefully, solutions of equation (4.21) will accurately predict the propagation of the fronts. We confirm that the slaving condition is met by observing in both figures that the numerically obtained curves for the temperature front position (the dashed curves) are seen to match closely with that of the numerically obtained electric field front position (the high frequency oscillating curve) during the initial (and remarkably linear) increase in the front positions. In both cases, the temperature front is seen to lag slightly behind the electric field front, as expected. This lag is most visible in Fig. 4, which is also expected to show the greatest lag because in this case the electric field is evolving fastest, while the rate of the temperature front propagation is roughly the same in both examples.

We next compare these curves with the corresponding prediction given by equation (4.27) for x_s^E and x_s^T. The latter are represented in the figures by the smooth solid monotonously increasing curve (recall that x_s^E and x_s^T are assumed to be equal (slaved)

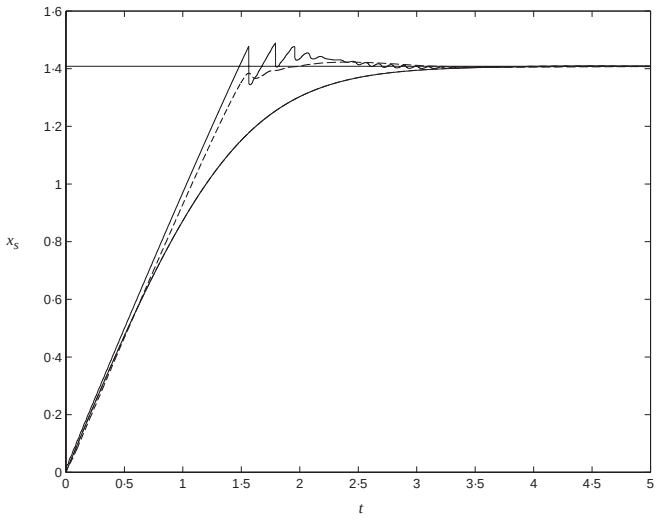

FIG. 5. Comparison of the numerical and analytical results for the relaxation of the electric and temperature fields to steady state; weak temperature dependence and large absolute electric conductivity. The values of parameters and curves are same as in Fig. 4, except the values $\sigma_0 = 2$, $\sigma_1 = 0{\cdot}2$.

in the foregoing analysis). For the prediction plotted in Fig. 4, the value $-2b$ was used for B in equation (4.27), which is permissible since σ_1 was small for this example. For the prediction in Fig. 5, three different values for the coefficient $\mathrm{Re}(A''/A')$ were employed. For the first two values, the values $-2b$ and the asymptotic value of expression (4.28) were used, and the curves were generated from equation (4.27) with B set equal to these values. In other simulations not presented here, equation (4.21) was solved numerically with $\mathrm{Re}(A''/A')$ given by equation (4.28).

We conclude that the analytical predictions for the electric field propagation appear to work quite well. In particular, we note that while the agreement is not absolutely perfect, the relaxation time scales and thermal front penetration depths in these examples are quite different, and this difference is much greater than the disagreement between analysis and simulation in each case, so that equation (4.21) appears to be doing a good overall job of predicting the time scale of the relaxation.

We also note that as the electric field approaches the steady state, the position of the electric field typically exhibits some oscillations. These oscillations are probably due to the fact that the Maxwell equation is of second order in time, and hence is capable of exhibiting 'inertial' oscillations, like those of a harmonic oscillator. During this stage, the temperature front is seen not to follow the electric field front very precisely. This discrepancy, which does not represent a significant failure in our predictions, is to be expected during this stage, because during this stage the *final* relaxation of the temperature front to steady state is very slow, as was explained at the beginning of the last section.

For completeness, we also remark that equation (4.21) fails to accurately predict the evolution of the fronts when ρ is small, that is, when condition $1/\rho \ll 1/(\sigma_0 + \sigma_1)$, is

violated. Solutions from numerical solutions of the full system and those given by (4.21) and (4.27), with values of $\rho = 1$, are found to be markedly different.

Where it is permissible to use $B = -2b$ in equation (4.27), we remark that the limit $\sigma_1 \to 0$ may be taken to obtain a prediction for the evolution of the electric field front with no coupling to temperature at all. The second example actually effectively demonstrates this, because σ_1 was negligible compared to σ_0 in this example. We therefore have apparently obtained some information about the relaxation to steady state in the Maxwell wave equation with *constant* conductivity, that is, for the Maxwell wave equation by itself, and thus the nonlinear ordinary differential equation (4·21) and its solution (4.27) may be of some wider interest than the main topic of the present study (thermal fronts).

5. Conclusions

We have explored some of the mathematical questions regarding the propagation of thermal fronts during electric volumetric heating in materials of low thermal diffusivity over a wide range of values of electric conductivity and, in the process, demonstrated how the FBP approximation (2.6)–(2.8) is useful for answering the questions posed in Section 1.2. Explicit expressions were obtained for field profiles at steady state, the location of the steady state, and for the relaxation dynamics of the fields, extending previous results by García-Reimbert *et al.* (1996).

Some of the same authors (Mercado and Xin) have found a rigorous proof of the existence of steady-state solutions of the free boundary problem by using the contraction mapping theorem in the regime of small σ_1 (see Mercado, 1999). We suggest that an even more extensive study might be possible to obtain a rigorous foundation for the asymptotic study of the time evolution of the original system and the stability of the solutions obtained.

Acknowledgements

The authors gratefully thank Mac Hyman and Regan E. Murray for many helpful discussions on the development of these results. Thanks also to The Center of Nonlinear Studies at Los Alamos National Laboratory for hosting Gema A. Mercado for the time in which part of this research was done. We also thank Catherine García-Reimbert and Tim Minzoni for leading us to this interesting problem and for their hospitality at the IIMAS-UNAM when Gema A. Mercado was a visitor in the winter of 2000. Another part of this work was done during a visit of Gema A. Mercado and Jack Xin to the Computational and Applied Math (CAM) division at UCLA in the summer of 1998. We thank the CAM faculty and staff for their hospitality and support, especially Professors R. Caflisch and S. Osher.

The research of the first author was supported by CONACYT Exp. SNI-21472; the work of the third was partially supported by NSF grant DMS-9625680.

References

BEATTY, R. L., SUTTON, W. H. & ISKANDER, M. F. (Eds) (1992) *Microwave Processing of Materials* III. Pittsburgh: Materials Research Society, 269.

CHEN, X. (1992) Generation and propagation of interfaces in reaction–diffusion systems. *Trans. Amer. Math. Soc.*, **334**, 877–913.

COLEMAN, C. J. (1991) On the microwave hotspot problem. *J. Austral. Math Soc.*, B **33**, 1–8.

FIFE, P. (1988) *Dynamics of Internal Layers and Diffusive Interfaces*, SIAM Regional Conference Series. Philadelphia: SIAM.

GARCÍA-REIMBERT, C., MINZONI, A. A. & SMYTH, N. F. (1996) Effect of radiation losses on hotspot formation and propagation in microwave heating. *IMA J. Appl. Math.*, **57**, 165–179.

HILL, J. M. & SMYTH, N. F. (1990) On the mathematical analysis of hotspots arising from microwave heating. *Math. Engng Industry*, **2**, 267–278.

KRIEGSMANN, G. A. (1997) Cavity effects in microwave heating of ceramics. *SIAM J. Appl. Math.*.

KRIEGSMANN, G. A. & VARATHARAJAH, P. (1993) Formation of hot spots in microwave heated ceramic roads. *Microwaves: Theory and Applications in Materials Processing* II, Ceramic Transactions 36. (D. E. Clark, W. R. Tinga & J. R Laia, eds). Westerville: The American Ceramic Society, pp. 382–400.

KRIEGSMANN, G. A., BRODWIN, M. E. & WATTERS, D. G. (1990) Microwave heating of a ceramic half space. *SIAM J. Appl. Math.*, **50**, 1088–1098.

MERCADO, G. A. (1999) *Hotspot dynamics in microwave heating*, Dissertation Thesis, Interdisciplinary Program in Applied Mathematics, University of Arizona.

MEREDITH, R. J. (1998) *Engineers' Handbook of Industrial and Microwave Heating*. The Institution of Electrical Engineers.

METAXAS, A. C. & MEREDITH, R. J. (1983) *Industrial Microwave Heating*, I.I.E. Power Engineering Series, 4. London: Perter Peregrimus.

PELESKO, J. A. & KRIEGSMANN, G. A. (1997) Microwave heating of ceramic laminates. *J. Engng Math.*, **32**, 1–18.

PINCOMBE, A. H. & SMYTH, N. F. (1991) Microwave heating of materials with low conductivity. *Proc. R. Soc.* A, **433**, 479–498.

SMYTH, N. F. (1990) Microwave heating of bodies with temperature dependent properties. *Wave Motion*, **12**, 171–186.

TIAN, Y. L. (1991) Practices of ultra-rapid sintering of ceramics using single mode applicators. *Microwaves: Theory and Practice in Microwave Processing*, Ceramic Transactions 21. (D. E. Clark, F. D. Gac & W. N Sutton, eds). Westerville: American Ceramic Society, pp. 283–300.

WATTERS, D. G. (1989) *An advanced study of microwave sintering*, Ph.D. Dissertation, Northwestern University.